7

Cherenkov Phase Matched Monochromatic Tunable Terahertz Wave Generation

Koji Suizu[1], Takayuki Shibuya[1,2] and Kodo Kawase[1,2]
[1]*Nagoya University,*
[2]*RIKEN*
Japan

1. Introduction

Terahertz (THz) waves present attractive possibilities in advanced applications including biomedical analysis and stand-off detection for hazardous materials. The development of monochromatic and tunable coherent THz-wave sources is of great interest for use in these applications. Recently, a parametric process based on second-order nonlinearities was used to generate tunable monochromatic coherent THz waves using nonlinear optical crystals (Boyd et al., 1972; Rice et al., 1994; Shi et al., 2002; Tanabe et al. 2003). In general, however, nonlinear optical materials have high absorption coefficients in the THz-wave region, which inhibits efficient THz-wave generation.

Avetisyan et al. proposed surface-emitting THz-wave generation using the difference frequency generation (DFG) technique in a periodically poled lithium niobate (PPLN) waveguide to overcome these problems (Avetisyan et al., 2002). A surface-emitted THz wave radiates from the surface of the PPLN and propagates perpendicular to the direction of the pump beam. The absorption loss is minimized because the THz wave is generated from the PPLN surface. Moreover, the phase-matching condition can be designed using PPLN with an appropriate grating period (Sasaki et al., 2002). Surface-emitted THz-wave devices have the potential for high conversion efficiency, and continuous wave THz-wave generation has been successfully demonstrated (Sasaki et al., 2005). Unfortunately, the tuning range of the THz waves is limited to about 100 GHz by the nature of PPLN, and a wide tuning range cannot be realized using the quasi-phase–matching method.

We developed a Cherenkov phase-matching method for monochromatic THz-wave generation using the DFG process with a lithium niobate crystal, which resulted in both high conversion efficiency and wide tunability. Although THz-wave generation by Cherenkov phase matching has been demonstrated using femtosecond pumping pulses (Auston et al., 1984; Kleinman et al., 1984; Hebling et al., 2002; Wahlstrand, 2003; Badrov et al., 2009), producing very high peak power (Yeh et al., 2007), these THz-wave sources are not monochromatic. Our method generates monochromatic and tunable THz waves using a nanosecond pulsed laser source.

2. Cherenkov phase matching

The Cherenkov phase-matching condition is satisfied when the velocity of the polarization wave inside the nonlinear crystal is greater than the velocity of the radiated wave outside.

Source: Recent Optical and Photonic Technologies, Book edited by: Ki Young Kim,
ISBN 978-953-7619-71-8, pp. 450, January 2010, INTECH, Croatia, downloaded from SCIYO.COM

The radiation angle θ is determined by the refractive index of the pumping wave in the crystal, n_{opt}, and that of THz-wave in the crystal, n_{THz} (Sutherland, 2003),

$$\cos\theta_{crystal} = \frac{\lambda_{THz}/n_{THz}}{2L_c} = \frac{\lambda_{THz}/n_{THz}}{\lambda_1\lambda_2/(n_1\lambda_2 - n_2\lambda_1)} \approx \frac{n_{opt}}{n_{THz}} \quad (1)$$

where λ is a wavelength of the contributing waves in the DFG process ($\omega_1 - \omega_2 = \omega_{THz}$), n_1, n_2 ($n_1=n_2\cong n_{opt}$) and n_{THz} are refractive index of the crystal at pump waves and THz-wave frequencies, respectively, and L_c is the coherence length of the surface-emitted process ($L_c = \pi/\Delta k$, where $\Delta k=k_1-k_2$ and k is the wave number). The Cherenkov angle, $\theta_{crystal}$, is determined by the refractive indices of the pumping wave and the THz-wave in the crystal, so the angle is strongly dependent on the choice of material. THz-frequency waves radiated at Cherenkov angles propagate to the crystal-air interface, and if the angle is greater than a critical angle (determined by the difference in refractive indices at the interface), the THz-frequency wave is totally reflected at the interface. To prevent total internal reflection, a clad material with a lower refractive index than that of the crystal in the THz range and a proper prism shape, is coupled in at the output. Figure 1 shows a schematic of Cherenkov radiation and output coupling of a THz-frequency wave.

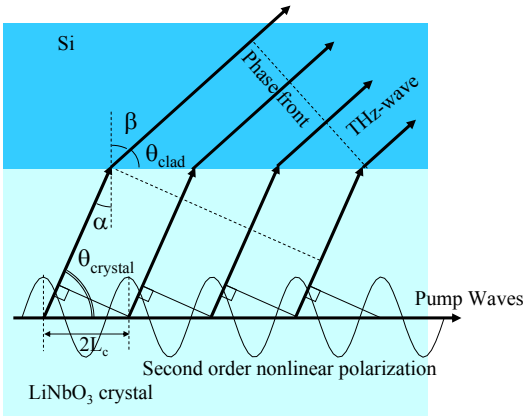

Fig. 1. Schematic of Cherenkov phase-matched monochromatic THz-wave generation.

Figure 2 shows relation of Cherenkov angle and critical angle of several clad materials. We choose polyethylene, diamond, Si and Ge as clad materials, because these materials have low absorbance and low dispersion character at THz frequency region. A total internal reflection occurs below the curve. For example, lithium niobate ($LiNbO_3$) has 2.2 and 5.2 of refractive index at near infrared and THz-wave region, results in 65 degree of Cherenkov angle in the crystal. On the other hands, critical angle of total internal reflection from the crystal to air, polyethylene, diamond, Si and Ge in a θ manner are 79, 76, 63, 49 and 40 degrees, respectively. The figure tells that diamond, Si and Ge prevent total internal reflection of Cherenkov radiation for lithium niobate crystal.

The angle in the clad material, θ_{clad}, is determined by Snell's law as shown in Fig. 1, using the refractive index of the clad material n_{clad}.

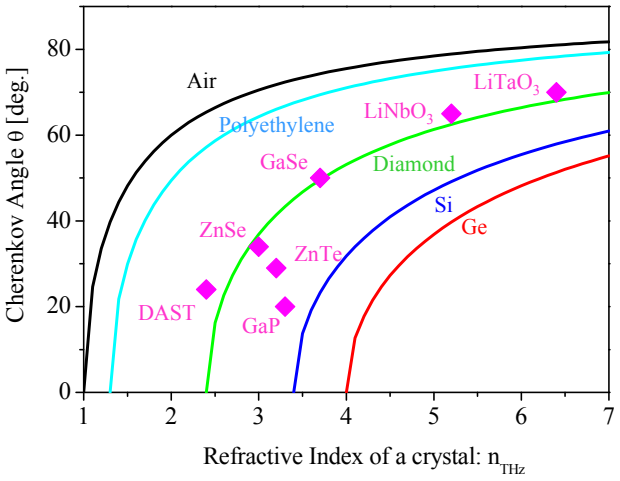

Fig. 2. Cherenkov angle for various nonlinear crystals (pink collared diamonds) and calculated critical angle between a crystal and a clad. Black, aqua, green, blue and red curve represent Air, polyethylene, diamond, Si and Ge as a clad material, respectively. A total internal reflection occurs below the curve.

$$\begin{aligned}\theta_{clad} &= \frac{\pi}{2} - \beta = \frac{\pi}{2} - \arcsin\left(\frac{n_{THz}}{n_{clad}}\sin(\alpha)\right) = \frac{\pi}{2} - \arcsin\left(\frac{n_{THz}}{n_{clad}}\sin\left(\frac{\pi}{2} - \theta_{crystal}\right)\right) \\ &= \frac{\pi}{2} - \arcsin\left(\frac{n_{THz}}{n_{clad}}\sin\left(\frac{\pi}{2} - \arccos\left(\frac{n_1\lambda_2 - n_2\lambda_1}{n_{THz}(\lambda_2 - \lambda_1)}\right)\right)\right) \\ &= \arccos\left(\frac{n_1\lambda_2 - n_2\lambda_1}{n_{clad}(\lambda_2 - \lambda_1)}\right)\end{aligned} \tag{2}$$

The radiation angle θ_{clad}, which is important for practical applications, is determined by the refractive indices of the pumping waves in the crystal and the THz-wave in the clad layer. Equation (2) is mathematically equivalent to a model in which the THz-wave is directly radiated to a clad layer. The equation tells us that n_{clad} should be larger than that of the nonlinear crystal in the pumping wave region. A comparison of the refractive indices of various nonlinear crystals with that of Si (about 3.4 in the THz-region) indicates that Si is an appropriate Cherenkov radiation output coupler for many crystals.

The radiation angle hardly changes during THz-frequency tuning because the silicon has low refractive index dispersion in the THz-wave region and the optical wavelength requires only slight tuning. The change in radiation angle is less than 0.01° for a fixed pumping wavelength. The actual angle change of the THz wave is significantly better than for the THz parametric oscillator (TPO) with a Si prism coupler (Kawase et al., 2001), which has an angle change of about 1.5° in the 0.7–3 THz tuning range.

3. Cherenkov phase-matched monochromatic THz-wave generation using difference frequency generation with a bulk lithium niobate crystal

3.1 Experimental setup

We demonstrated the method described above using the experimental setup shown in Fig. 3 (Suizu et al. 2008). The frequency-doubled Nd:YAG laser, which has pulse duration of 15 ns, a pulse energy of 12 mJ when operating at 532 nm, and a repetition rate of 50 Hz, was used as the pump source for a dual-wavelength potassium titanium oxide phosphate (KTP) optical parametric oscillator (OPO). The KTP-OPO, which consists of two KTP crystals with independently controlled angles, is capable of dual-wavelength operation with independent tuning of each wavelength (Ito et al., 2007). The OPO has a tunable range of 1300 to 1600 nm. The maximum output energy of 2 mJ was obtained for a pumping energy of less than 12 mJ. The 5 mol% MgO-doped lithium niobate crystal (MgO:$LiNbO_3$) used in the experiment was cut from a 5 × 65 × 6 mm wafer, and the x-surfaces at both ends were mirror-polished. An array of seven Si prism couplers was placed on the y-surface of the MgO:$LiNbO_3$ crystal. The y-surface was also mirror-polished to minimize the coupling gap between the prism base and the crystal surface, and to prevent scattering of the pump beam, which excites a free carrier at the Si prism base. To increase the power density, the pump beam diameter was reduced to 0.3 mm. The polarizations of the pump and THz waves were both parallel to the Z-axis of the crystals. The THz-wave output was measured with a fixed 4 K Si bolometer.

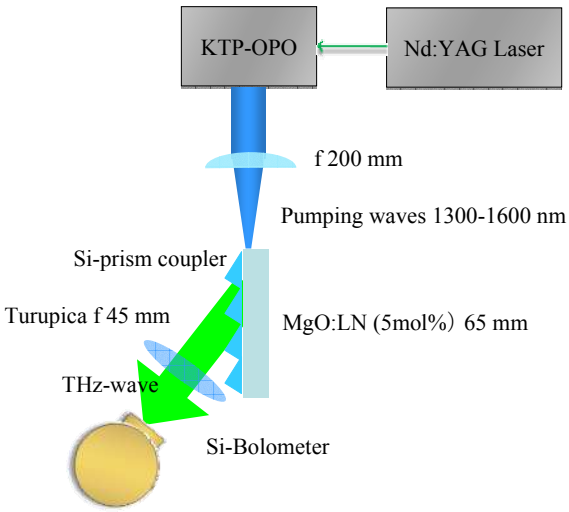

Fig. 3. Experimental setup for Cherenkov phase-matching monochromatic THz-wave generation with a bulk lithium niobate crystal.

3.2 Results and discussions

The THz-wave output map for various pumping wavelengths and corresponding THz-wave frequencies is shown in Fig. 4. The magnitude of the map denotes the output voltage of a Si bolometer with a gain of 200. The noise level of the bolometer was about 10 mV and is shown as the blue region in the figure. The regions where over 2 V of output voltage were

obtained is red. As seen in the figure, wide tunability in the range 0.2–3.0 THz was obtained by choosing the proper pumping wavelength. Especially for lower frequency below 1.0 THz, this was very efficient compared to our previous TPO systems that used 1470 nm pumping.

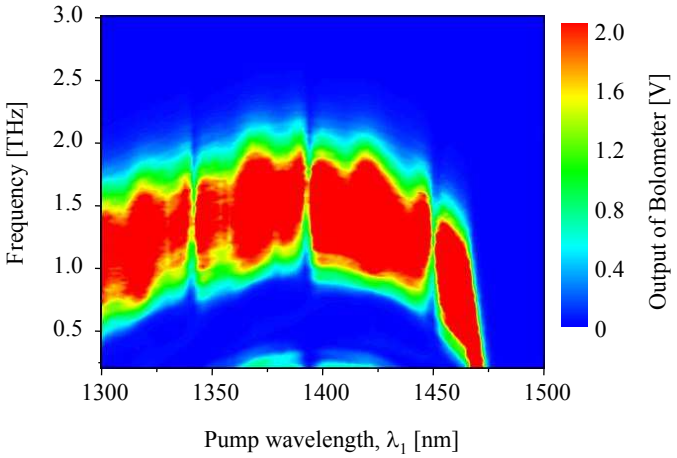

Fig. 4. THz-wave output mapping for various pumping wavelengths and corresponding THz-wave frequencies. The X-axis and Y-axis denote pumping wavelength λ_1 and THz-wave frequency, respectively. The magnitude of the map values indicates the output voltage of the detector.

Figure 5 (a) shows cross sections of the THz-wave output map of Fig. 4. The highest THz-wave energy obtained was about 800 pJ, using the fact that 1 V ≈ 101 pJ/pulse for low repetition rate detection, pulsed heating of the Si device, and an amplifier gain of 200 at the bolometer, and the energy conversion efficiency from the λ_1 wave (1 mJ/pulse) was about 10^{-4}%. This value is comparable to that obtained with our previous TPO systems, despite the low excitation energy of only 1 mJ. The figures clearly show the strong dependence of THz-wave output energy on the pumping wavelength. In the case of 0.8 THz generation, the output energy had a dip at a pumping wavelength of approximately 1400 nm as shown in Fig. 5(a). We obtained extremely high energy in the low-frequency region below 0.3 THz (millimeter wave region) using 1470 nm pumping. The reason for this is not clear, and the dispersion of pumping waves cannot explain the results; thus, an explanation is left for future research. The important result is that we could obtain a flat output spectrum in the range 0.2–2 THz by choosing proper pumping wavelength, as shown in Fig. 5(b).

Cherenkov phase matching inherently requires a waveguide structure for nonlinear polarization waves in the crystal to suppress phase mismatching in the direction perpendicular to the guiding mode (i.e., normal to the crystal surface). If we reduce the width of the pumping beams in the direction of THz-wave propagation to about one-half of the THz wavelength, (i.e., about 10 μm for 3 THz) by taking into account the refractive index of MgO:$LiNbO_3$ in the THz-wave region, no need exists to consider phase matching in that direction (Suizu et al., 2006). In our case, the waist of the pump beams in the MgO:$LiNbO_3$ was about 300 μm, which corresponds to about five cycles of THz waves at 1.0 THz, and one cycle of THz waves at 0.2 THz. Although the experimental conditions did not satisfy the requirement for Cherenkov phase matching, we did successfully detect Cherenkov-radiated

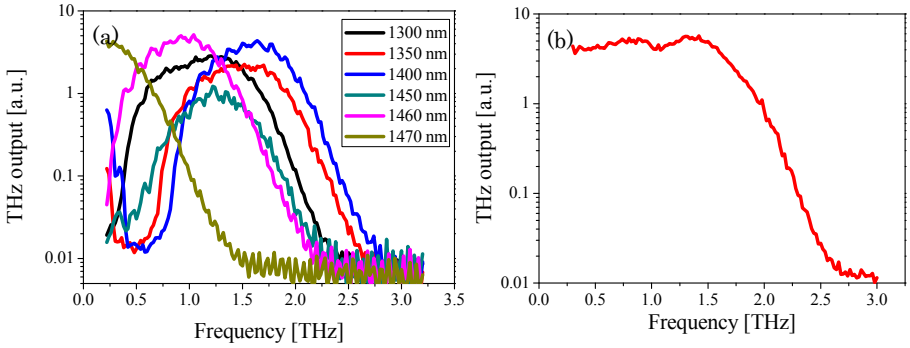

Fig. 5. THz-wave spectra (a) at various pumping wavelength and (b) under choosing proper pumping wavelengths.

THz waves, which originated in the higher absorbance area of the crystal at the THz-wave region. The THz waves generated far from the crystal surface would be attenuated and no significant phase mismatch would occur. This also remains an area for future study.
By shaping the pumping beams with a focused cylindrical lens or by adopting the waveguide structure of the crystal, we could neglect phase mismatches and obtain a higher power density of the pumping beams, resulting in higher conversion efficiency.

4. Efficient Cherenkov-type phase-matched widely tunable THz-wave generation via an optimized pump beam shape

We demonstrated the Cherenkov-type phase-matching method for monochromatic THz-wave generation via the DFG process using bulk lithium-niobate crystal. We successfully generated monochromatic, widely tunable THz waves in the 0.2- to 3.0-THz range. We obtained efficient energy conversion in the low-frequency region below 0.5 THz and achieved a flat tuning spectrum by varying the pumping wavelength during THz-wave tuning. The highest THz-wave energy was about 800 pJ pulse^{-1}, which was obtained for a broad spectral region in the range of 0.2 to 2.0 THz. However, obtaining high conversion efficiency in the frequency domain above 2 THz was difficult, and the output was almost zero at 3 THz. The output of the THz wave decreased in the high-frequency region due to a phase mismatch incurred by the finite size of the pumping beam diameter. As shown in Fig. 6(b), Cherenkov-type phase matching arises due to a superposition of spherical THz waves from the nonlinear polarization maxima created by pumping lights of two different frequencies in the NLO crystal, and thus, when the finite beam size is taken into account, the phase shift of the wave depends on the distance from the y-surface of the crystal. THz waves generated far from the crystal surface destructively interfere with those generated in the neighbourhood of a crystal surface. The beam diameter of the pumping wave in a lithium-niobate crystal in our previous work was about 300 μm, corresponding to about the wavelength of the THz wave at 0.2 THz, and ten cycles of THz waves at 2.0 THz, as the refractive index of lithium niobate is about 5.2. Since the 300-μm beam diameter is over 15 times the wavelength of a THz wave above the 3-THz region, a phase mismatch occurred

and the THz-wave output decreased. In this experiment, we attempted to improve the THz-wave generation efficiency above 3 THz by optimizing the beam shape of the pumping wave to decrease the beam-diameter dependence effect (Shibuya et al., 2009).

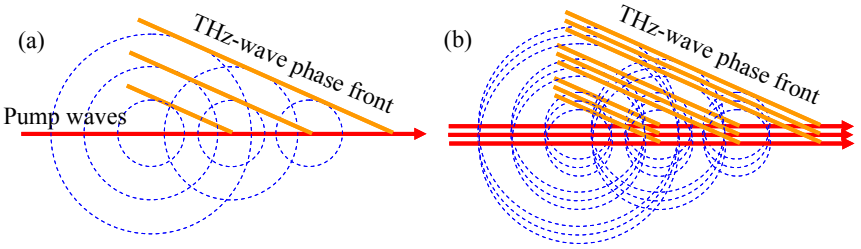

Fig. 6. (a) Ideal Cherenkov-type phase-matching condition; (b) Cherenkov-type phase-matching condition when the beam diameter of the exciting light is considered. In (b), the phase mismatch is caused by the finite size of the beam diameter.

4.1 Experimental setup

A dual-wavelength potassium titanium oxide phosphate (KTP) optical parametric oscillator (OPO) with a pulse duration of 15 ns, a pulse energy of 1.6 mJ, a 50-Hz repetition rate, and a tunable range of 1300 to 1600 nm was used for a DFG pumping source. The size of the MgO-doped lithium-niobate crystal was 5×65×6 mm^3. We used cylindrical lenses to reduce the pump beam diameter. The focal lengths of the cylindrical lenses were 20, 50, 100, and 150 mm, and the beam widths parallel to the crystal's y-axis were 35, 46, 83, and 127 μm (FWHM), respectively. The pump power was adjusted, and the power density on the focus position was made constant at 200 MW cm^{-2} for all lenses.

The obtained THz-wave output spectrum is shown in Fig. 7. The vertical axis is the THz-wave pulse energy calculated from the output voltage of a Si-bolometer detector. The horizontal axis is the THz-wave frequency. THz-wave output spectra were measured by selecting the excitation wavelength in which the maximum output was obtained for each THz-wave frequency. The output in the high-frequency region increased as the focal length of the cylindrical lens decreased. THz-wave generation was confirmed over the 3-THz region with the 20-mm and 50-mm cylindrical lenses. The tunable range for the 20-mm cylindrical lens was about 0.2 to 4 THz. This is the widest tuning range for the previous lithium-niobate crystal-generated THz-wave source. The pumping-wave beam diameter in the lithium-niobate crystal using the 20-mm cylindrical lens was about 35 μm, which corresponded to about 1.8-THz wave cycles at 3 THz. The phase mismatch is thought to have decreased as the beam diameter decreased, leading to an output improvement in the high-frequency region. Meanwhile, the conversion efficiency decreased because the pumping-wave beam diameter corresponded to over 2.3-THz wave cycles and the absorption coefficient increased rapidly above 4 THz. The absorption coefficient of the crystal at 4 THz was 425 cm^{-1}. When the pump beam moved 100 μm away from the y-surface of the crystal, 98.6% of the output was lost. Additionally, narrowing the beam diameter further was difficult due to diffraction. As the beam diameter narrowed, the confocal length shortened and the conversion efficiency decreased. The low-frequency region generation efficiency was expected to decrease for the 20-mm cylindrical lens case because the confocal length shortened. This problem can be prevented by using a

waveguiding structure. By limiting the beam diameter of the pump wave to half of the wavelength using only the waveguide mode for THz-wave generation, the phase mismatch can be neglected and absorption loss reduced. This is because the distance from the y-surface to the pump beam drops to almost zero, causing a higher conversion efficiency and a wider spectrum.

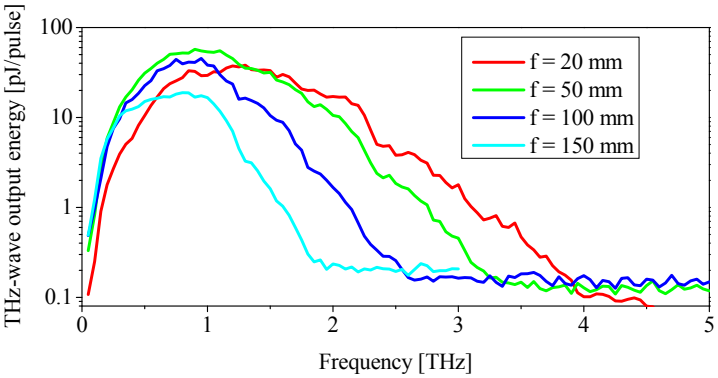

Fig. 7. THz-wave output spectra obtained using various cylindrical lenses, as measured by selecting the excitation wavelength in which the maximum output was obtained for each THz-wave frequency.

5. Extremely frequency-widened Cherenkov-Type Phase-Matched terahertz wave generation with a lithium niobate waveguide

Here, we show that Cherenkov radiation with waveguide structure is an effective strategy for achieving efficient and extremely wide tunable THz-wave source (Suizu et al., 2009). We fabricated MgO-doped lithium niobate slab waveguide with 3.8 μm of thickness and demonstrated difference frequency generation of THz-wave generation with Cherenkov phase matching. Extremely frequency-widened THz-wave generation, from 0.1 to 7.2 THz, without no structural dips successfully obtained. The tuning frequency range of waveguided Cherenkov radiation source was extremely widened compare to that of injection seeded-Terahertz Parametric Generator. The tuning range obtained in this work for THz-wave generation using lithium niobate crystal was the widest value in our knowledge. The highest THz-wave energy obtained was about 3.2 pJ, and the energy conversion efficiency was about 10^{-5} %. The method can be easily applied for many conventional nonlinear crystals, results in realizing simple, reasonable, compact, high efficient and ultra broad band THz-wave sources.

5.1 Experimental setup

Here, we prepared a slab waveguide of a lithium niobate crystal. A Y-cut 5 mol % MgO-doped lithium niobate crystal on a thick congruent lithium niobate substrate was polished down to 3.8 μm. A thin MgO-doped lithium niobate layer worked as an optical slab waveguide, because the refractive indexes of 5 mol % MgO-doped lithium niobate and congruent lithium niobate at 1300 nm are 2.22 and 2.15, respectively. The waveguide device

was 5-mm wide and 70-mm long (X-axis direction). Each X-surface facet was mechanically polished to obtain an optical surface. We demonstrated difference-frequency generation using the experimental setup shown in Fig. 8(b). A dual-wavelength potassium titanium oxide phosphate (KTP) optical parametric oscillator (OPO) with a pulse duration of 15 ns, a pulse energy of 1 mJ and a 1300- to 1600-nm tunable range was used as a pumping source. A thin (3.4-μm thick) polyethylene terephthalate (PET) film was slipped between the array of Si prism couplers and the Y-surface of the MgO-doped lithium niobate crystal. Directly placing an array of Si prism couplers on the Y-surface of the MgO-doped lithium niobate will inhibit the function of the MgO-doped lithium niobate layer as a waveguide for pumping waves, because the refractive index of Si in the near-infrared region is higher (about 3.5) than that of lithium niobate (about 2.2). A PET, in contrast, has a lower refractive index in that region (about 1.3), so adding a thin PET film does not inhibit the function of the crystal as a waveguide. An array of Si prism couplers on a PET film can work as a coupler for THz-frequency waves, because the PET film is thin compared to the wavelength of a THz-frequency wave. A schematic of the coupling system of the pumping wave and THz-wave emitting system is shown in Fig. 8(a). To couple pumping waves, the pump beam was reduced to few micrometers in the X-axis direction by a 3-mm diameter glass rod lens. The width of the pumping beams in the Z-direction was about 1.9 mm. The waveguide power density was about 53 MW cm^{-2}, estimated from the pump wave pulse energy after waveguide propagation (about 60 μJ). We did not observe or calculate the waveguide mode of the structure in which a thin MgO-doped lithium niobate layer was sandwiched by a thick congruent lithium niobate layer and a thin PET film. It remains an area of future work to optimize the waveguide structure. The pump wave and THz-frequency wave polarizations were parallel to the crystal's Z-axis. The THz-wave output was measured with a fixed 4-K Si bolometer.

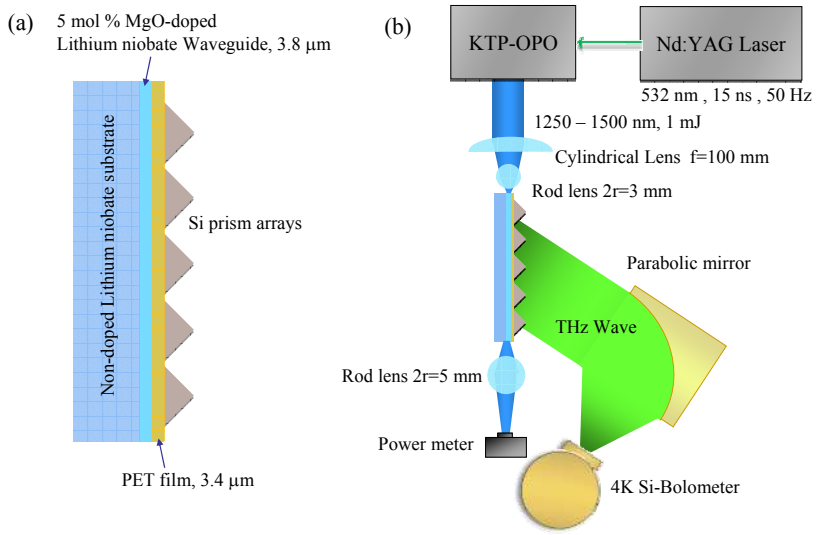

Fig. 8. (a) Schematic of the lithium niobate waveguide device with Si prism array coupler. (b) THz-wave detection experimental setup.

Figure 9 shows a THz-wave spectrum at various wavelength of λ_1 from 1250 to 1350 nm. The spectrum was obtained by varying λ_2 at fixed λ_1. As shown in Fig. 9, high-frequency THz-wave output ranging to about 7.2 THz was confirmed. We were unable to observe THz-wave generation around 7.2 THz due to very strong THz-wave absorption at 7.5 THz by the LO-phonon mode. The THz-wave spectrum does not depend on pumping wavelength because the near-infrared refractive index is almost constant in the 1250- to 1350-nm range.

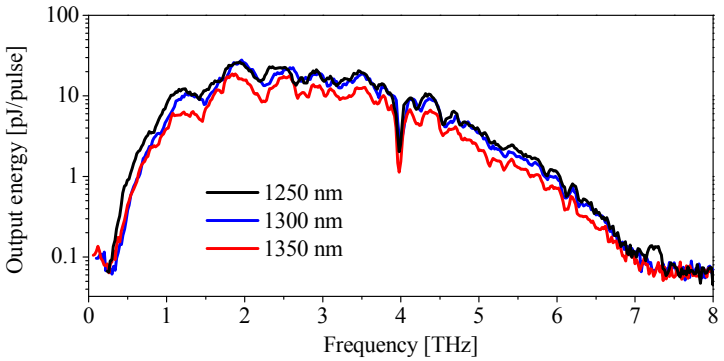

Fig. 9. THz-frequency spectrum of waveguided Cherenkov radiation. Black, red, blue and green curves represent pumping wavelengths of 1250, 1300, 1350 nm, respectively.

Figure 10 shows a comparison of normalized tuning spectrum of the waveguided Cherenkov radiation source and injection seeded terahertz parametric generator (is-TPG) (Kawase et al., 2002). Nevertheless each THz source were based on a same nonlinear crystal, MgO-doped lihitum niobate, a tuning frequency range of waveguided Cherenkov radiation source was extremely widened compare to that of is-TPG. We converted the output voltage of the Si bolometer to the actual THz-wave energy, using the fact that 1 V ≈ 20 pJ pulse^{-1} for low repetition rate detection, pulsed heating of the Si device, and an amplifier gain of 1000 at the bolometer. The highest THz-wave energy obtained was about 28 pJ, and the energy conversion efficiency from the λ_1 wave (30 μJ pulse^{-1}) was about 10^{-4}%. This value is comparable to our previous work on Cherenkov radiation using bulk crystal, despite the low excitation energy of only 30 μJ. The tuning range obtained in this work for THz-wave generation using lithium niobate crystal was the widest value in our knowledge.

The THz-wave emitting angle was absolutely constant, as Si dispersion in this range is almost flat. The device would be work well in an optical rectification process using a femtosecond laser. Such a range, free from structural dips between 0.1 and 7.2 THz, is suitable for ultra-short pulse generation. Also, the surface emission process used here is loss-less, permitting the generation of a continuous, widely-tunable THz-frequency range, and requiring only two easily commercially available diode lasers. Compact, robust and reasonable THz-wave sources can be realized by this method. Although we demonstrated this method using only a lithium niobate crystal, it can be adopted for other nonlinear crystals, such as $LiTaO_3$, GaSe, GaP, ZnSe, ZnTe, ZGP, DAST and so on. By choosing the best clad materials for the nonlinear crystals (in many case Si or Ge), the Cherenkov

condition is easily satisfied, and control of crystal angles to satisfy phase-matching conditions, such as birefringence phase-matching, is not required. This method opens the door to simple, reasonable, compact, highly efficient and ultra-broadband THz-wave sources.

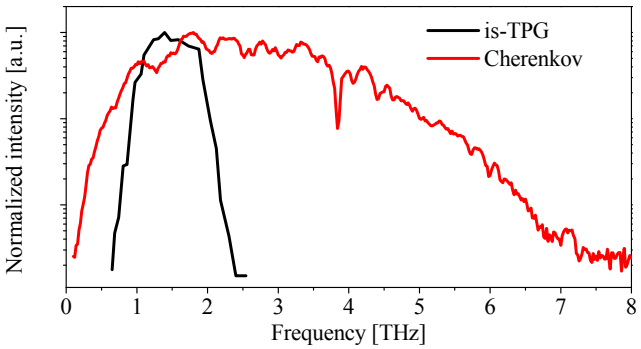

Fig. 10. A comparison of normalized tuning spectrum of the waveguided Cherenkov radiation source under 1250 nm pumping (red curve) and is-TPG (black curve).

6. Cherenkov phase matched THz-wave generation with surfing configuration for bulk Lithium Niobate crystal

We demonstrated a Cherenkov phase matched THz-wave generation with surfing configuration for bulk lithium niobate crystal (Suizu et al., 2009). THz-wave output was enhanced about 50 times by suppressing phase mismatching for THz-wave propagation direction. The suppression was achieved by combining two pumping waves with dual wavelength with finite angle, and THz-frequency was controllable by changing the angle within 2.5 degrees range. Higher frequency THz-wave generation at around 4.0 THz was successfully obtained by the method.

6.1 Cherenkov phase mating with surfing configuration

We demonstrated Cherenkov phase matching method for monochromatic THz-wave generation via DFG process using bulk lithium niobate crystal. We successfully generated monochromatic THz-waves with wide tunability in the range 0.2–2.5 THz. The highest THz-wave energy was about 800 pJ/pulse, and this energy could be obtained for the broad spectral region in the range around 0.2–2.0 THz. Although we successfully got wide tunable characteristics of THz-wave generation, conversion efficiency of a THz-wave generation at higher frequency region above 2.0 THz was slightly low. It would be caused by phase mismatch of generated THz-wave in a propagating direction of THz-wave. Beam diameter of pumping waves in a lithium niobate crystal in our previous work was about 300 μm, which corresponded to about ten cycles of THz waves at 2.0 THz because the refractive index of lithium niobate is about 5.2. THz-wave generated at far from a crystal surface interfered with that generated at neighborhood of a crystal surface, resulted in denying each other. By reducing the width of beam diameter in the crystal in the direction of THz-wave propagation to about one-half of the THz wavelength, there was no need to consider phase matching in that direction. We observed the effects by condensing a pump beam diameter to a THz-wave propagation direction by cylindrical lenses. Although higher THz-wave around

4.0 THz was successfully generated under tight focusing by the cylindrical lens with 20 mm of focus length, output of THz-wave at lower frequency region was reduced, because tight focusing resulted in reducing interaction length for pumping wave propagating direction.
In this study, we propose surfing configuration of Cherenkov type phase matching for THz-wave generation for bulk crystal to suppress a phase mismatching. Interference pattern of pumping waves in the crystal is induced by combining the dual wavelengths beams with finite angle. It provides a same spatial pattern of second order nonlinear polarization in THz-frequency. The interference pattern has not checkerboard one, which is a results of interference of tilted beams with same frequency, because dual wavelength beam courses other spatial interference pattern, corresponding to difference frequency, and the interference pattern is superimposed in checkerboard one.
Figure 11 shows electric field distribution of (a) pumping waves and (b) excited nonlinear polarization, with λ_1=1300 nm, λ_2=1317 nm (here, three waves in DFG interaction has a relation of $\omega_1=\omega_2-\omega_{THz}$, and corresponding THz frequency is 3 THz) and 3.7 degrees of angle between divided pumping beams, α. The periods of nonlinear polarization pattern of dual wavelengths beams, A for x-axis and B for y-axis are represented by following equations,

$$A=\frac{2\pi}{(k_1-k_2)\cos\frac{\alpha}{2}},\ B=\frac{4\pi}{(k_1+k_2)\sin\frac{\alpha}{2}} \tag{3}$$

where $k_1=2\pi n_1/\lambda_1$ and $k_2=2\pi n_2/\lambda_2$, here n_1 and n_2 are refractive index of λ_1 and λ_2, respectively. We used Sellmeier equation at near-infrared region for a lithium niobate crystal (Jundt, 1997). On the other hands, Cherenkov angle of the crystal, θ_c, is decided by relation of length A and THz-wavelength in the crystal, $C=\lambda_{THz}/n_{THz}$, here λ_{THz} and n_{THz} are THz-wavelength in vacuum and refractive index of the crystal at THz frequency. A phase matching condition for THz-wave propagation direction is satisfied by choosing an appropriate angle α of the pump beams for required THz-frequency. The angle α is formulated from geometric relation of A, B and C, $A^2C^2=B^2C^2=A^2B^2$, as shown in Fig.11(c).

$$\alpha=2\arccos\left(\sqrt{\frac{-(k_1+k_2)^2+\frac{16\pi^2}{(\lambda_{THz}/n_{THz})^2}}{4(k_1-k_2)^2-(k_1+k_2)^2}}\right) \tag{4}$$

Generated THz-wave can propagate without influence of phase mismatching in the direction of propagating direction, just like as surf rider on nonlinear polarization waves, as shown in Fig.11 (b). The required angle for frequency tuning was shown in Fig.12 (a) internal and (b) external crystal. Phase matching condition is satisfied by changing the angle α for required THz-wave and pumping wave wavelength. And slightly narrow tunability (about 300 GHz at around 3 THz generation) is obtained at a fixed angle, α=4.0 degrees.

6.2 Experimental setup

Figure 13 shows the schematic of experimental setup. A pump source for DFG process was same as our previous works, and which has a tunable range of 1250 to 1500 nm, 15 ns of pulse duration and 0.88 mJ of pulse energy. An output of the source with dual wavelength

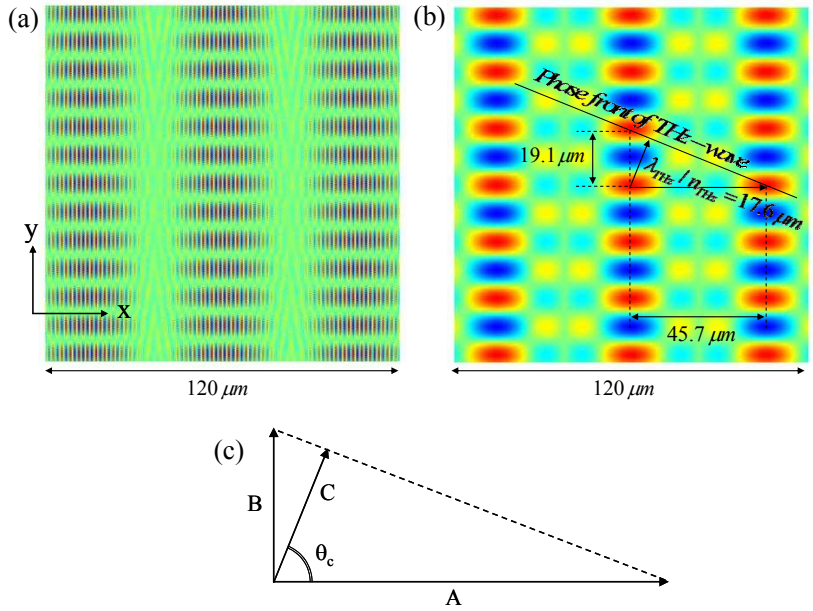

Fig. 11. Normalized electric field distribution of (a) combined dual wavelength pump beams with finite angle, and (b) exited second order nonlinear polarization of difference frequency. Here, λ_1=1300 nm, λ_2=1317 nm and 3 THz of difference frequency with 3.7 degrees of beam angle. (c) Geometric relation of A: excited nonlinear polarization for x-direction, B: interference period of pump beams for y-direction and C: THz-wavelength in the crystal.

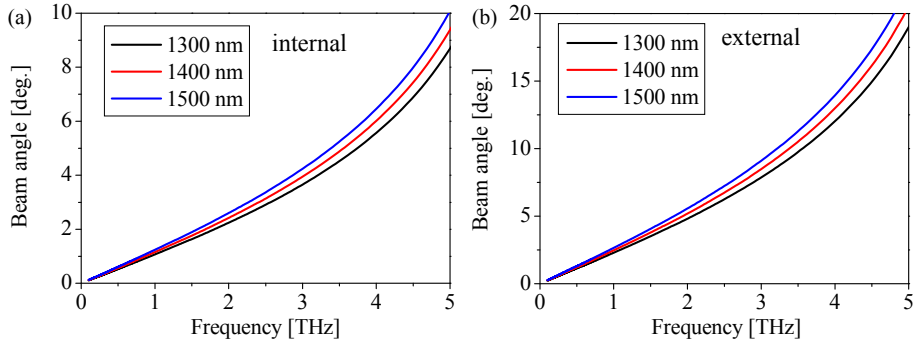

Fig. 12. Tuning angle (a) internal and (b) external of crystal under 1300, 1400 and 1500 nm of pumping wavelength of λ_1.

was focused by circular lens (f=500 mm) before divided by half beam splitter, and combined again with finite angle. The spot diameter of the combined beam was 0.45 mm. The 5 mol % MgO-doped lithium niobate crystal (MgO:$LiNbO_3$) used in the experiment was cut from a 5

× 65 × 6 mm wafer. The polarizations of the pump and THz waves were both parallel to the Z-axis of the crystals. The THz-wave output was measured with a fixed 4 K Si bolometer.

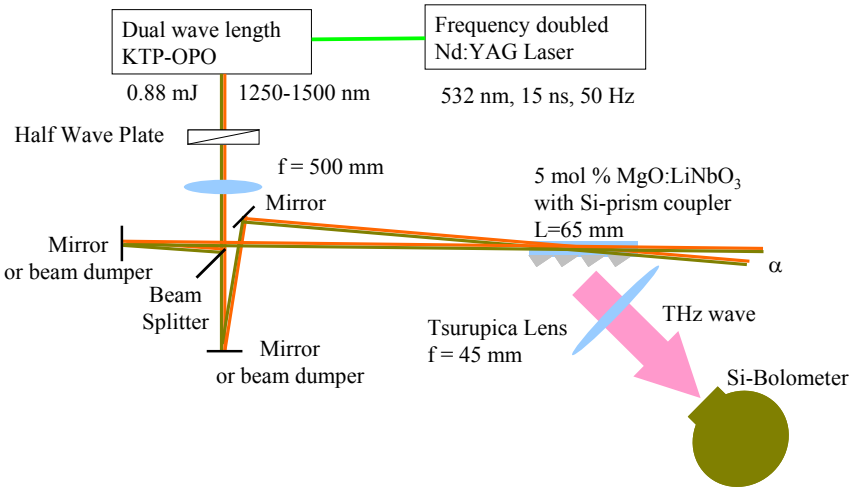

Fig. 13. Schematic of experimental setup for Cherenkov phase matching THz-wave generation with surfing configuration.

6.3 Results and discussions

Input-output properties of THz-wave for pumping energy are shown in Fig.14 at 1.0 THz generation with α=2.49 degrees. Circles and triangles denotes THz-wave output signal with combined beams and with single beam by dumping the other beam before entrance to the crystal, respectively. Maximum pumping energy of only 0.44 mJ was achieved at single beam pumping, because a half of whole pumping energy was dumped as shown in Fig.13. The vertical axis is the THz-wave pulse energy calculated from the output voltage of a Si-bolometer detector, a pulse energy of about 101 pJ/pulse corresponded to a Si-bolometer voltage output of 1 V when the repetition rate was less than 200 Hz. As shown in the figure, remarkable enhancement of THz-wave generation with surfing configuration, whose magnetic was about 50 times, was successfully observed. Inset of Fig.14 shows double logarithmic plot of input-output properties. Slope efficiency under combined beams and single beam pumping were almost same values. It means that enhancement factor of about 50 was a result of a suppression of phase miss-matching.

The generated THz-waves at different position in the crystal were in-phase each other, and outputted THz-wave was enhanced. Intensity of overlapping in-phase THz-waves in an absorptive media was calculated as shown in Fig.15. A 5 mol % MgO-doped Lithium Niobate crystal at THz-wave frequency region would has about 30 cm^{-1} of absorption coefficient (Palfalvi et al., 2005). The enhancement effect of in-phase interference would be effective for about 2 mm of traveling distance of THz-wave, this fact leads optimum pumping beam width in y-axis direction is about 1.8 mm. In this study, pumping beam width in y-axis was about 0.45 mm, results in a propagating length of a THz-wave was about 1.2 mm. Higher enhancement above 50 would be obtained with tight focused beam only for z-axis by cylindrical lens.

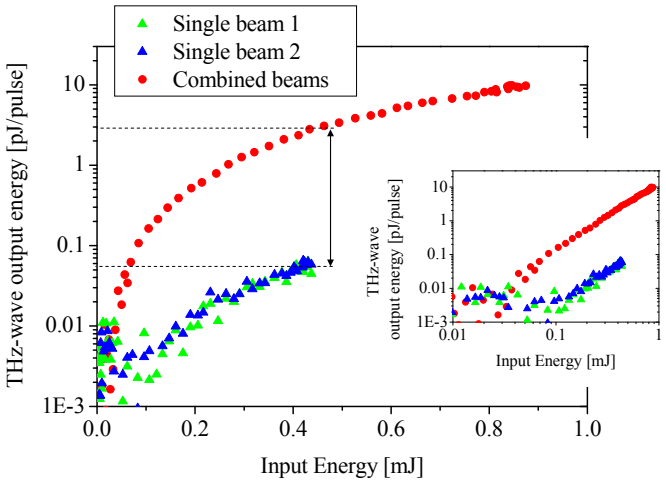

Fig. 14. Input-output property of THz-wave for pumping energy at 1.0 THz generation with α=2.49 degrees. Circles and triangles denotes THz-wave output signal with combined beams and with single beam. Inset shows double logarithmic plot of input-output properties.

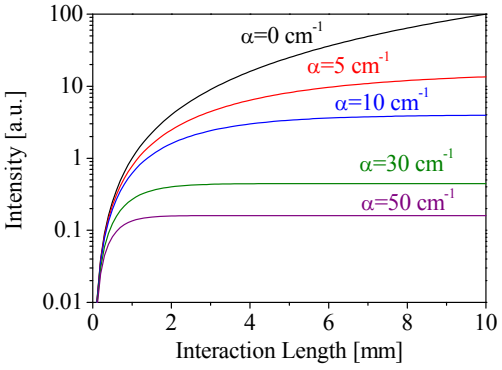

Fig. 15. Calculated intensity of overlapping in-phase THz-waves in an absorptive media.

Figure 16 shows THz-wave output characteristics under fixed pumping wavelength of 1300 nm and several fixed angle, 2.49, 3.80 and 5.03 degrees. Maximum THz-wave output at each angle was obtained at higher frequency in the bigger angle, α. Obtained peaks of THz-wave output were about 1.1, 1.6 and 1.9 THz, respectively. The relation between the angle and the frequency where maximum output was obtained agree well with Equation 4, 1.08, 1.61 and 2.07 THz under 1300 nm pumping respectively. Tuning range for higher frequency region was remarkably improved compare with our previous collinear and not tight focused configuration. THz-wave output at around 4 THz was successfully obtained.

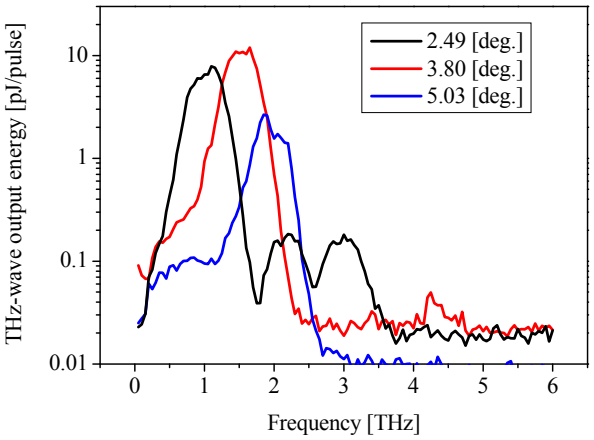

Fig. 16. THz-wave output spectra under fixed pumping wavelength of 1300 nm and several fixed angle, 2.49, 3.80 and 5.03 degrees.

As described in our previous work, because the linewidth of each pumping wave is about 60 GHz, the source linewidth is about 100 GHz, which is slightly broader than that obtained from sources such as injection-seeded terahertz parametric generator (Kawase et al., 2002) or DAST crystal-based difference-frequency generators (Powers et al., 2005). This occurs because the linewidth of the THz-wave depends on that of the pumping source.

The spectrum with α=2.49 degrees pumping had two dips at 1.8 and 2.6 THz. It coursed by perfect phase miss-matching of THz-wave propagation. Figure 17 shows calculated nonlinear polarization distributions at (a) 1.8 and (b) 2.6 THz generation with α=2.49. THz-wavelength in the crystal at 1.8 THz generation is 32.2 μm. Generated THz-wave at point "a" in Fig.17 interferes with that at point "b", which has a phase difference by π compare to that of point "a", results in destructive interference. Similarly, and adding higher order interference, generated THz-wave at point "c" has destructive interference with that at point "d". THz-wave generation was observed at around the dips, because perfect phase miss-matching was relaxed at these frequencies. We have not yet completed the analytical solution predicting the frequency due to destructive interference, and it remains an area of future work.

Broader tuning range would be obtained by controlling the angle α within about only 2.5 degrees range. Because lithium niobate is strongly absorbing at THz-frequencies, the beam-crossing position was set near the crystal surface to generate the THz-wave. In this configuration, the pumping beam passing through a Si prism yields an optical carrier excitation in Si that prevents THz-wave transmission, while the interaction length decreases at larger pumping angles, α. The interaction lengths,

$$l = 2D / \tan\alpha \tag{5}$$

where D is the beam diameter, are 21.4 and 10.7 mm for αs of 2.49° and 5.03°, respectively. If we use a shorter lithium niobate crystal, the optical carrier excitation can be avoided, and larger pumping angles can be employed to obtain higher-frequency generation. The method is

very simple way to obtain higher frequency and efficient generation of THz-wave, because the method does not require a special device such as slab waveguide structure.

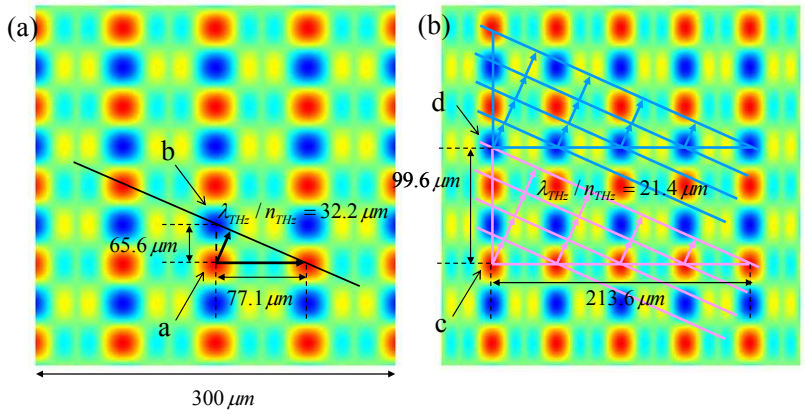

Fig. 17. Calculated nonlinear polarization distributions at (a) 1.8 and (b) 2.6 THz generation with α=2.49.

7. References

Auston, D. H.; Cheung, K. P.; Valdmanis, J. A. & Kleinman, D. A. (1984). Cherenkov radiation from femtosecond optical pulses in electro-optic media. *Phys. Rev. Lett.* 53, 1555–1558.

Avetisyan, Y.; Sasaki, Y. & Ito, H. (2001). Analysis of THz-wave surface-emitted difference-frequency generation in periodically poled lithium niobate waveguide. *Appl. Phys.* B 73, 511–514.

Bodrov, S. B.; Stepanov, A. N.; Bakunov, M. I.; Shishkin1, B. V.; Ilyakov, I. E. & Akhmedzhanov, R. A. (2009). Highly efficient optical-to-terahertz conversion in a sandwich structure with $LiNbO_3$ core. *Opt. Express* 17, 1871-1879.

Boyd, G. D.; Bridges, T. J.; Patel, C. K. N. & Buehler, E. (1972). Phase-matched submillimeter wave generation by difference-frequency mixing in $ZnGeP_2$. *Appl. Phys. Lett.* 21, 553–555.

Hebling, J.; Almasi, G.; Kozma, I. & Kuhl, J. (2002). Velocity matching by pulse front tilting for large area THz-pulse generation. *Opt. Express* 10, 1161–1166.

Ito, H.; Suizu, K.; Yamashita, T. & Sato, T. (2007). Random frequency accessible broad tunable terahertz-wave source using phase-matched 4-dimethylamino-N-methyl-4-stilbazolium tosylate (DAST) crystal. *Jpn. J. Appl. Phys.* 46, 7321–7324.

Jundt, D. H. (1997). Temperature-dependent sellmeier equation for the index of refraction, ne, in congruent lithium niobate. *Opt. Lett.* 22, 1553-1555.

Kawase, K.; Shikata, J.; Minamide, H.; Imai, K. & Ito, H. (2001). Arrayed silicon prism coupler for a terahertz-wave parametric oscillator. *Appl. Opt.* 40, 1423-1426.

Kawase, K.; Minamide, H.; Imai, K.; Shikata, J. & Ito, H. (2002). Injection-seeded terahertz-wave parametric generator with wide tenability. *Appl. Phys. Lett.* 80, 195-197.

Kleinman, D. A. & Auston, D. H. (1984). Theory of electro-optic shock radiation in nonlinear optical media. *IEEE J. Quantum Electron.* 20, 964–970.

Palfalvi, L.; Hebling, J.; Kuhl, J.; Peter, A. & Polgar, K. (2005). Temperature dependence of the absorption and refraction of Mg-doped congruent and stichiometric $LiNbO_3$ in the THz range. *J. Appl. Phys*. 97, 123505.

Powers, P. E.; Alkuwari, R. A.; Haus, J. W.; Suizu, K. & Ito, H. (2005). Terahertz generation with tandem seeded optical parametric generators. *Opt. Lett.* 30, pp. 640-642.

Rice, A.; Jin, Y.; Ma, X. F.; Zhang, X. C.; Bliss, D.; Larkin, J. & Alexander, M. (1994). Terahertz optical rectification from <110> zinc-blende crystals. *Appl. Phys. Lett.* 64, 1324–1326.

Sasaki, Y.; Avetisyan, Y.; Kawase, K. & Ito, H. (2002). Terahertz-wave surface-emitted difference frequency generation in slant-stripe-type periodically poled $LiNbO_3$ crystal. *Appl. Phys. Lett.* 81, 3323–3325.

Sasaki, Y.; Avetisyan, Y.; Yokoyama, H. & Ito, H. (2005). Surface-emitted terahertz-wave difference frequency generation in two-dimensional periodically poled lithium niobate. *Opt. Lett.* 30, 2927–2929.

Sasaki, Y.; Yokoyama, H. & Ito, H. (2005). Surface-emitted continuous-wave terahertz radiation using periodically poled lithium niobate. *Electron. Lett.* 41, 712–713.

Shi, W.; Ding, Y. J.; Fernelius, N. & Vodopyanov, K. (2002). Efficient, tunable, and coherent 0.18–5.27-THz source based on GaSe crystal. *Opt. Lett.* 27, 1454–1456.

Shibuya, T.; Tsutsui, T.; Suizu, K.; Akiba, T. & Kawase, K. (2009). Efficient Cherenkov-Type Phase-Matched Widely Tunable THz-Wave Generation via an Optimized Pump Beam Shape. *Appl. Phys. Express* 2, 032302.

Suizu, K.; Suzuki, Y.; Sasaki, Y.; Ito, H. & Avetisyan, Y. (2006). Surface-emitted terahertz-wave generation by ridged periodically poled lithium niobate and enhancement by mixing of two terahertz waves. *Opt. Lett.* 31, 957-959.

Suizu, K.; Tutui, T.; Shibuya, T.; Akiba, T. & Kawase, K. (2008). Cherenkov phase-matched monochromatic THz-wave generation using difference frequency generation with lithium niobate crystal. *Opt. Express* 16, 7493-7498.

Suizu, K.; Koketsu, K.; Shibuya, T.; Tsutsui, T.; Akiba, T. & Kawase, K. (2009). Extremely frequency-widened terahertz wave generation using Cherenkov-type radiation. *Optics Express*, 17, 6676-6681.

Suizu, K.; Tsutsui, T.; Shibuya, T.; Akiba, T. & Kawase, K. (2009). Cherenkov phase-matched THz-wave generation with surfing configuration for bulk lithium niobate crystal. *Optics Express*, 17, 7102-7109.

Sutherland, R. L. (2003). *Handbook of Nonlinear Optics*, Chap. 2. Marcel Dekker, New York.

Tanabe, T.; Suto, K.; Nishizawa, J.; Saito, K. & Kimura, T. (2003). Tunable terahertz wave generation in the 3- to 7-THz region from GaP. *Appl. Phys*. Lett. 83, 237–239.

Wahlstrand J. K. & Merlin, R. (2003). Cherenkov radiation emitted by ultrafast laser pulses and the generation of coherent polaritons. *Phys. Rev.* B 68, 054301.

Yeh, K.-L.; Hoffmann, M. C.; Hebling, J. & Nelson, K. A. (2007). Generation of 10 μJ ultrashort THz pulses by optical rectification. *Appl. Phys. Lett.* 90, 171121.

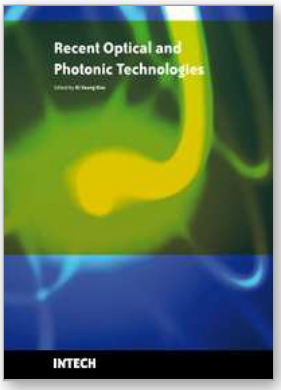

Recent Optical and Photonic Technologies

Edited by Ki Young Kim

ISBN 978-953-7619-71-8
Hard cover, 450 pages
Publisher InTech
Published online 01, January, 2010
Published in print edition January, 2010

Research and development in modern optical and photonic technologies have witnessed quite fast growing advancements in various fundamental and application areas due to availability of novel fabrication and measurement techniques, advanced numerical simulation tools and methods, as well as due to the increasing practical demands. The recent advancements have also been accompanied by the appearance of various interdisciplinary topics. The book attempts to put together state-of-the-art research and development in optical and photonic technologies. It consists of 21 chapters that focus on interesting four topics of photonic crystals (first 5 chapters), THz techniques and applications (next 7 chapters), nanoscale optical techniques and applications (next 5 chapters), and optical trapping and manipulation (last 4 chapters), in which a fundamental theory, numerical simulation techniques, measurement techniques and methods, and various application examples are considered. This book deals with recent and advanced research results and comprehensive reviews on optical and photonic technologies covering the aforementioned topics. I believe that the advanced techniques and research described here may also be applicable to other contemporary research areas in optical and photonic technologies. Thus, I hope the readers will be inspired to start or to improve further their own research and technologies and to expand potential applications. I would like to express my sincere gratitude to all the authors for their outstanding contributions to this book.

How to reference

In order to correctly reference this scholarly work, feel free to copy and paste the following:

Koji Suizu, Takayuki Shibuya and Kodo Kawase (2010). Cherenkov Phase Matched Monochromatic Tunable Terahertz Wave Generation, Recent Optical and Photonic Technologies, Ki Young Kim (Ed.), ISBN: 978-953-7619-71-8, InTech, Available from: http://www.intechopen.com/books/recent-optical-and-photonic-technologies/cherenkov-phase-matched-monochromatic-tunable-terahertz-wave-generation

INTECH
open science | open minds

InTech Europe
University Campus STeP Ri
Slavka Krautzeka 83/A
51000 Rijeka, Croatia
Phone: +385 (51) 770 447
Fax: +385 (51) 686 166

InTech China
Unit 405, Office Block, Hotel Equatorial Shanghai
No.65, Yan An Road (West), Shanghai, 200040, China
中国上海市延安西路65号上海国际贵都大饭店办公楼405单元
Phone: +86-21-62489820
Fax: +86-21-62489821